Eur. Phys. J. Plus (2016) **131**: 282
DOI 10.1140/epjp/i2016-16282-4

THE EUROPEAN PHYSICAL JOURNAL PLUS

Regular Article

Interacting new holographic dark energy in dynamical Chern-Simons modified gravity

Abdul Jawad[a], Shamaila Rani[b], and Tanzeela Nawaz[c]

Department of Mathematics, COMSATS Institute of Information Technology, Lahore - 54000, Pakistan

Received: 4 April 2016 / Revised: 12 July 2016
Published online: 19 August 2016 –

Abstract. In this paper, we explore various cosmological parameters (equation of state, squared speed of sound, Om-diagnostic) and cosmological planes (ω_ϑ-ω'_ϑ, where ω'_ϑ is the evolutionary equation of state parameter, statefinder). We consider the framework of dynamical Chern-Simons modified gravity with the new holographic dark energy model. It is observed that the equation of state parameter gives consistent ranges by using different observational schemes. We check the stability of the model using the squared speed of sound. In the present scenario, the squared speed of sound shows a stable solution. The ω_ϑ-ω'_ϑ and statefinder planes also present consistent results. We would like to mention here that our results of cosmological parameters show consistency with previous different observational data like Planck, H_0, SNLS and WMAP.

1 Introduction

Astronomers with the help of various observational analyses, such as SNIa, SDSS, WMAP and CMB radiation, and X-ray, have suggested that our universe undergoes accelerated expansion [1–7]. On the basis of these observations, they also argued that our universe is spatially flat and consists of about 70% dark energy (DE) with negative pressure, 30% dust matter (cold dark matter plus baryons) and negligible radiation. But the nature of DE is still ambiguous and requires more attention. Up to now, two distinct scenarios have been designed, such as dynamical DE models and modified theories of gravity. The family of Chaplygin gas [8,9], holographic DE (HDE) [10–12], pilgrim DE [13–18], etc., lie in the category of dynamical DE models which are mostly used in describing the cosmological scenario.

The HDE model is one of the most fascinating DE models, which has been constructed in the framework of quantum gravity through the holographic principle [19]. In the derivation of this DE model, the black hole entropy plays a key role. In view of black hole entropy relation, Cohen *et al.* [20] have suggested a relation according to which the total energy of the system with size L should not exceed the mass of a black hole with the same radius. For the largest value of L to saturate this process, the energy density of HDE is given by

$$\rho_\vartheta = 3n^2 m_{pl}^2 L^{-2}, \tag{1}$$

where n, m_{pl} and L are the numerical constant, reduced Planck mass and IR cutoff, respectively. For illustrating the cosmic acceleration in a more reliable way, various IR cutoffs have been developed, such as the Hubble radius, event horizon, the age of the universe, Granda-Oliveros (GO) length, Ricci length, etc. In the Kaluza-Klein universe, Sharif and Jawad [21] analyzed the interaction of modified HDE and dark matter with varying G. They considered infrared cutoff scale L as future event horizon. In this scenario, the EoS parameter as well as its evolution are explored. They also checked the validity of the generalized second law of thermodynamics. This model represents the transition of the universe from quintessence to phantom and showed consistency with the present observations.

[a] e-mail: abduljawad@ciitlahore.edu.pk
[b] e-mail: shamailatoor.math@yahoo.com
[c] e-mail: tanzeela_nawaz@yahoo.com

On the other hand, various modified gravities have also been suggested for explaining cosmic acceleration. Among them, the Chern-Simons modified gravity has been developed recently [22] and was not a random extension. This gravity is motivated by string theory (as a necessary anomaly-canceling term to conserve unitarity [23]) as well as by loop quantum gravity [24]. This modified gravity exhibits the violation of parity symmetry in Einstein-Hilbert action because of the inclusion of the Pontryagin density (a topological term in four dimensions, unless the coupling constant is not constant or promoted to a scalar field). The detail of this modified gravity has been given in [25]. Many authors have investigated cosmic acceleration in the dynamical Chern-Simons modified gravity by taking various HDE models [26–30].

To realize the role of DE in modified gravity, a very useful technique is proposed by [31–35] and also extended for several cosmological scenarios. There exist several DE EoSs in the literature, however, the authors of [34] have discussed the more general forms of DE inhomogeneous EoS. In view of these EoSs, they have usefully remarked that the more general form may contain the derivative of H, like $\dot{H}, \ddot{H}, \ldots$, in principle, and it is given by

$$F(p, \rho, H, \dot{H}, \ddot{H}) = 0.$$

This form contains a family of Chaplygin gas and much more complicated EoSs. The interested feature of this form, as addressed by Nojiri *et al.* [34], is that one can recover Friedmann equations through its trivial condition. They have also investigated its non-trivial scenario and sketched a useful picture of cosmological implications. They pointed out that the inhomogeneous term in the EoS helps to realize the crossing of phantom barrier. They have also discussed the future behavior of the universe through singularity analysis by taking the several specific examples of the above general form of EoS.

In this paper, we consider HDE with the GO cut-off in the framework of dynamical Chern-Simons modified gravity. We explain the cosmological scenario, such as EoS parameter, Om-diagnostic, stability analysis, ω_ϑ-ω'_ϑ plane, statefinder plane. We analyzed the results by comparing with the observational data. The paper is organized as follows. In sect. 2, we briefly discuss the Chern-Simon modified gravity and the HDE model with the GO cutoff. In sect. 3, we discuss the cosmological parameters. Section 4 is about the cosmological planes. Finally, we will conclude with our results.

2 Basic equations

The action which describes the Chern-Simons theory is defined as follows [26–29]:

$$S = \frac{1}{16\pi G}\int \mathrm{d}^4x \left[\sqrt{-g}R + \frac{\ell}{4}\theta {}^\star R^{\rho\sigma\mu\nu}R_{\rho\sigma\mu\nu} - \frac{1}{2}g^{\mu\nu}\nabla_\mu\theta\nabla_\nu\theta + V(\theta)\right] + S_{\mathrm{mat}}. \tag{2}$$

Here, R, ${}^\star R^{\rho\sigma\mu\nu}R_{\rho\sigma\mu\nu}$, ℓ, θ, S_{mat} and $V(\theta)$ represent the Ricci scalar, a topological invariant called the Pontryagin term, the coupling constant, the dynamical variable, the action of matter and the potential, respectively. We set $V(\theta) = 0$ for simplicity. By varying the action equation (2) with respect to $g_{\mu\nu}$ and scalar field θ, we can get field equations as follows:

$$\begin{aligned} G_{\mu\nu} + \ell C_{\mu\nu} &= 8\pi G T_{\mu\nu}, \\ g^{\mu\nu}\nabla_\mu\nabla_\nu\theta &= -\frac{\ell}{64\pi}{}^\star R^{\rho\sigma\mu\nu}R_{\rho\sigma\mu\nu}, \end{aligned} \tag{3}$$

respectively. Here, $G_{\mu\nu}$ and $C_{\mu\nu}$ represent the Einstein and Cotton tensors, respectively. The Cotton tensor is defined as follows:

$$C^{\mu\nu} = -\frac{1}{2\sqrt{-g}}((\nabla_\rho\theta)\varepsilon^{\rho\beta\tau(\mu}\nabla_\tau R^{\nu)}_{\beta}) + (\nabla_\sigma\nabla_\rho\theta)^\star R^{\rho(\mu\nu)\sigma}. \tag{4}$$

In this framework, the energy-momentum tensors have the following forms:

$$\begin{aligned} \hat{T}^\theta_{\mu\nu} &= \nabla_\mu\theta\nabla_\nu\theta - \frac{1}{2}g_{\mu\nu}\nabla^\rho\theta\nabla_\rho\theta, \\ T_{\mu\nu} &= (\rho + p)u_\mu u_\nu + p g_{\mu\nu}, \end{aligned} \tag{5}$$

where $\hat{T}^\theta_{\mu\nu}$ and $T_{\mu\nu}$ corresponds to scalar field and energy densities contributions, respectively, while ρ and p represent the energy density (due to DE and CDM), pressure (due to only DE component), respectively. Moreover, $u_\mu = (1, 0, 0, 0)$ is the four-velocity. Using eqs. (3) and (5), we get the following Friedmann equation for flat universe:

$$H^2 = \frac{1}{3}(\rho_m + \rho_\vartheta) + \frac{1}{6}\dot{\theta}^2, \tag{6}$$

where $H = \frac{\dot{a}}{a}$ is the Hubble parameter, dot denotes the derivative of scale factor a with respect to cosmic time and $m_{pl}^{-1} = 8\pi G = 1$.

Now let us take the scalar field associated in eq. (4) which takes the following form for the FRW metric:

$$g^{\mu\nu}\nabla_\mu\nabla_\nu\theta = g^{\mu\nu}[\partial_\mu\partial_\nu\theta] = 0. \tag{7}$$

Choosing $\theta = \theta(t)$, we get the following equation:

$$\ddot{\theta} + 3H\dot{\theta} = 0 \;\Rightarrow\; \dot{\theta} = ba^{-3}, \tag{8}$$

where b is a constant of integration. Substituting this result into eq. (6), we obtain that

$$H^2 = \frac{1}{3}(\rho_m + \rho_\vartheta) + \frac{b^2a^{-6}}{6}\,. \tag{9}$$

Since we consider the interacting scenario of DE and CDM, the continuity equation turns out to be

$$\dot{\rho}_m + 3H\rho_m = \Gamma, \tag{10}$$

$$\dot{\rho}_\vartheta + 3H\rho_\vartheta(1+\omega_\vartheta) = -\Gamma. \tag{11}$$

There Γ shows the interaction term which is dynamical in nature. For simplicity, we take the following form of interaction term:

$$\Gamma = 3\gamma^2 H\rho_m, \tag{12}$$

where γ^2 is the interaction parameter which transfers the energy between CDM and DE. Using this result in eq. (10),

$$\rho_m = \rho_{m0}a^{-3(1-\gamma^2)}. \tag{13}$$

Finally, we consider HDE with the Granda-Oliveros cutoff (which is also called new HDE model). This cutoff has been proposed by Granda and Oliveros [12] who introduced a new IR cutoff, by including a term proportional to $\dot{H}$ and one term proportional to H^2,

$$L = (\alpha\dot{H} + \beta H^2), \tag{14}$$

where α and β represent two constant parameters. The expression of the HDE energy density with this cutoff is given by

$$\rho_\vartheta = 3(\alpha\dot{H} + \beta H^2). \tag{15}$$

3 Cosmological parameters

In this section, we study the cosmological parameters, such as the EoS parameter, the stability analysis and Om-diagnostic. By using eq. (15) into eq. (9), we get the differential equation in terms of Hubble parameter as

$$\dot{H} = \frac{1-\beta}{\alpha}H^2 - \frac{H_0^2\Omega_{m0}}{\alpha}a^{-3(1-\gamma^2)} - \frac{1}{6\alpha}b^2a^{-6}. \tag{16}$$

Taking $x = \ln a$ in eq. (16), we get the solution

$$H^2 = \frac{2H_0^2\Omega_{m0}e^{-3(1-\gamma^2)x}}{(3\alpha(1-\gamma^2)+2(1-\beta))} + \frac{b^2e^{-6x}}{18\alpha+6(1-\beta)} + c_1e^{\frac{2(1-\beta)x}{\alpha}}\,, \tag{17}$$

where c_1 is the constant of integration and other constants parameters are $H_0 = 74$, $\Omega_{m0} = 0.23$, respectively.

3.1 EoS parameter

The EoS parameter can be obtained with the help of eqs. (11), (12) and (15) as follows:

$$\omega_\vartheta = -1 + \frac{1}{3\rho_\vartheta}\left[9H_0^2\gamma^2\Omega_{m0}e^{-3(1-\gamma^2)x} - \rho'_\vartheta\right]. \tag{18}$$

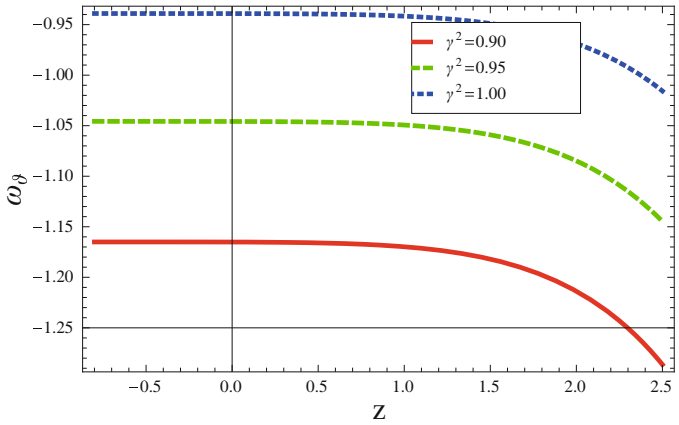

Fig. 1. Plots of the EoS parameter *versus* z.

The derivative of ρ_ϑ takes the form

$$\rho'_\vartheta = 3b^2 e^{-6x}\left(1-\frac{2}{6\alpha+2(1-\beta)}\right)\frac{6e^{\frac{2x(1-\beta)}{\alpha}}(1-\beta)}{\alpha}c_1 - 9(1-\gamma^2)e^{-3(1-\gamma^2)x} \times\left(-1+\frac{2}{3(1-\gamma^2)\alpha+2(1-\beta)}\right)H_0^2\Omega_{m0}. \tag{19}$$

Inserting the value of ρ'_ϑ in eq. (18) we obtain that

$$\omega_\vartheta = -1-\left[9H_0^2\Omega_{m0}\left(\frac{2}{3(1-\gamma^2)\alpha+2(1-\beta)}-1\right)e^{-3x(1-\gamma^2)}+9c_1e^{\frac{2x(1-\beta)}{\alpha}} -\frac{3b^2}{2}\left(\frac{-2}{6\alpha+2(1-\beta)}+1\right)e^{-6x}\right]^{-1}\left[9H_0^2\gamma^2\Omega_{m0}e^{-(1-\gamma^2)x}-3b^2e^{-6x} \times\left(1-\frac{2}{6\alpha+2(1-\beta)}\right)\frac{6e^{\frac{2x(1-\beta)}{\alpha}}c_1}{\alpha}+\left(-1+\frac{2H_0\Omega_{m0}}{3(1-\gamma)\alpha+2(1-\beta)}\right) \times 9(1-\gamma^2)e^{-(1-\gamma^2)x}\right].$$

The plot of ω_ϑ *versus* z for some constant cosmological parameters is shown in fig. 1. We use some specific values of parameters, such as $\Omega_{mo}=0.27$, $H_0=74$, $c_1=-1$, $b=3$ respectively. It can be seen that the EoS parameter lies in the phantom region for all values of the interacting parameter γ^2. Moreover, the constraints on the EoS parameter has also been developed through a combination of various observational data at the 95% confidence level by the Planck Collaboration ([6] and references therein). The detail is as follows:

$$\begin{aligned}
&\omega_\vartheta = -1.13^{+0.24}_{-0.25} \quad \text{(Planck+WP+BAO)},\\
&\omega_\vartheta = -1.09\pm 0.17 \quad \text{(Planck+WP+Union 2.1)},\\
&\omega_\vartheta = -1.13^{+0.13}_{-0.14} \quad \text{(Planck+WP+SNLS)},\\
&\omega_\vartheta = -1.24^{+0.18}_{-0.19} \quad \text{(Planck+WP+}H_0\text{)}.
\end{aligned}$$

In the present case, the EoS parameter (fig. 1) shows consistency with the above observational results.

3.2 The stability analysis

The stability analysis in the present framework is being discussed in this section. For this purpose, we extract the following squared speed of sound:

$$v_s^2 = \frac{\dot{p}}{\dot{\rho}} = \frac{p'}{\rho'} = \frac{p'_\vartheta}{\rho'_\vartheta},$$

Inserting corresponding expressions and after some calculations, we obtain the squared speed of sound as follows:

$$
\begin{aligned}
v_s^2 = -1 - \Bigg(& \frac{-3b^2e^{-6x}(3\alpha-\beta)}{1+3\alpha-\beta}\,\frac{6e^{\frac{-2x(-1+\beta)}{\alpha}}c_1}{\alpha} + 9\gamma^2 e^{3(-1+\gamma^2)x}H_0^2\Omega_{m0} \\
& + \frac{9(-1+\gamma^2)e^{3(-1+\gamma^2)x}(3(-1+\gamma^2)\alpha+2\beta)H_0^2\Omega_{m0}}{3(-1+\gamma^2)\alpha+2(-1+\beta)}\Bigg)\Bigg(\frac{-3b^2e^{-6x}}{2(1+3\alpha-\beta)} \\
& + (3\alpha-\beta)9e^{\frac{-2x(-1+\beta)}{\alpha}}c_1 + 9e^{3(-1+\gamma^2)x}\left(-1+\frac{2}{2-3(-1+\gamma^2)\alpha-2\beta}\right) \\
& \times H_0^2\Omega_{m0}\Bigg)^{-1} + \Bigg[-\frac{3(-1+\gamma^2)e^{3(-1+\gamma^2)x}(3(-1+\gamma^2)\alpha+2\beta)H_0^2\Omega_{m0}}{3(-1+\gamma^2)\alpha+2(-1+\beta)} \\
& + 9\left(\frac{b^2e^{-6x}(3\alpha-\beta)}{1+3\alpha-\beta} - \frac{2e^{\frac{2x(-1+\beta)}{\alpha}}(-1+\beta)}{\alpha}\right)\left(\frac{-3b^2e^{-6x}(3\alpha-\beta)}{1+3\alpha-\beta}\right. \\
& + \frac{6e^{\frac{-2x(-1+\beta)}{\alpha}}(-1+\beta)c_1}{\alpha} + 9\gamma^2e^{3(-1+\gamma^2)x}H_0^2\Omega_{m0} + 9(-1+\gamma^2)e^{3(-1+\gamma^2)x} \\
& \times\left.\left(3(-1+\gamma^2)\frac{(\alpha+2\beta)H_0^2\Omega_{m0}}{3(-1+\gamma^2)\alpha+2(-1+\beta)}\right)\right)\Bigg]\Bigg[\left(\frac{-3b^2e^{-6x}(3\alpha-\beta)}{2(1+3\alpha-\beta)}+9\right. \\
& \times e^{\frac{-2x(-1+\beta)}{\alpha}}c_1 + 9e^{3(-1+\gamma^2)x}\left(-1+\frac{2H_0^2\Omega_{m0}}{2-3(-1+\gamma^2)\alpha}-2\beta\right)\Bigg)^{-2} \\
& \times\left(\frac{3b^2e^{-6x}3\alpha-\beta}{3\alpha-\beta} - \frac{6e^{\frac{-2x(-1+\beta)}{\alpha}}(-1+\beta)c_1}{\alpha} - (3(-1+\gamma^2)\alpha+2\beta)H_0^2\Omega_{m0}\right. \\
& \times\left.\frac{9(-1+\gamma^2)e^{3(-1+\gamma^2)x}}{3(-1+\gamma^2)\alpha+2(-1+\beta)}\right)^{-1}\Bigg] - \Bigg[3\left(\frac{b^2e^{-6x}(-3\alpha+\beta)}{2(1+3\alpha-\beta)} + 3e^{\frac{-2x(-1+\beta)}{\alpha}}c_1\right. \\
& + \left.3e^{3(-1+\gamma^2)x}\left(-1+\frac{2H_0^2\Omega_{m0}}{2-3(-1+\gamma^2)(\alpha-2\beta)}\right)\right)\left(\frac{6b^2e^{-6x}(3\alpha-\beta)}{1+3\alpha-\beta} - 4e^{\frac{-2x(1+\beta)}{\alpha}}\right. \\
& \times\left.\frac{(-1+\beta)^2c_1}{\alpha^2} + \frac{9(-1+\gamma^2)^2e^{3(-1+\gamma^2)x}(3(-1+\gamma^2)\alpha2\beta)H_0^2\Omega_{m0}}{3(-1+\gamma^2)\alpha+2(-1+\beta)}\right) \\
& + 9d^2(-1+\gamma^2)e^{3(-1+\gamma^2)x}H_0^2\Omega_{m0}\Bigg]\Bigg[\frac{-3b^2e^{-6x}(3\alpha-\beta)}{2(1+3\alpha-\beta)} + 9e^{\frac{-2x(-1+\beta)}{\alpha}}c_1 \\
& + 9e^{3(-1+\gamma^2)x}\left(-1+\frac{2}{2-3(-1+\gamma^2)\alpha-2\beta}\right)H_0^2\Omega_{m0}\Bigg]^{-1}.
\end{aligned}
$$

The squared speed of sound exhibits the stability of the model for $v_s^2 > 0$, while instability of the model for $v_s^2 < 0$. In the present case, the squared speed of sound displayed against z for different values of γ^2 is shown in fig. 2. We can observe that the squared speed of sound shows the stability of the model at the present epoch as well as the later epoch.

3.3 Om-diagnostic

The Om-diagnostic [36] is another tool to discriminate different phases of the universe. It is also used to distinguish the ΛCDM for non-minimally coupled scalar field, phantom field and generic quintessence model through trajectories of the curves involving in the plot. The positive trajectory of $Om(x)$ implies that the DE era is like phantom ($\omega_\vartheta < -1$), whereas the negative trajectory means that DE constitutes quintessence ($\omega_\vartheta > -1$). The Om-diagnostic in terms of x function is defined as

$$Om(x) = \frac{\frac{H^2(x)}{H_0} - 1}{x^3 - 1}\,.$$

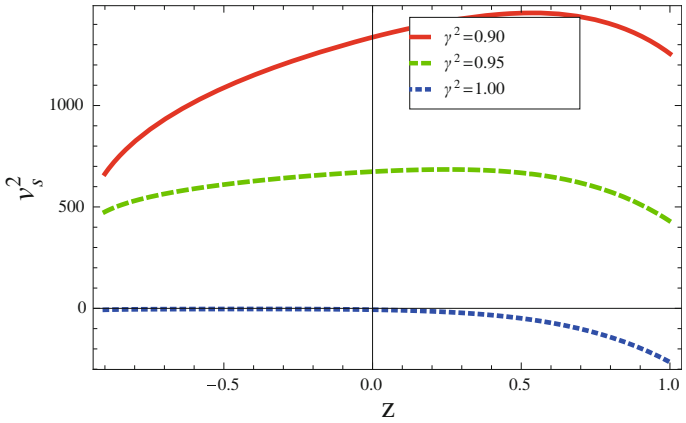

Fig. 2. Plots of the stability analysis with the squared speed of sound *versus* z.

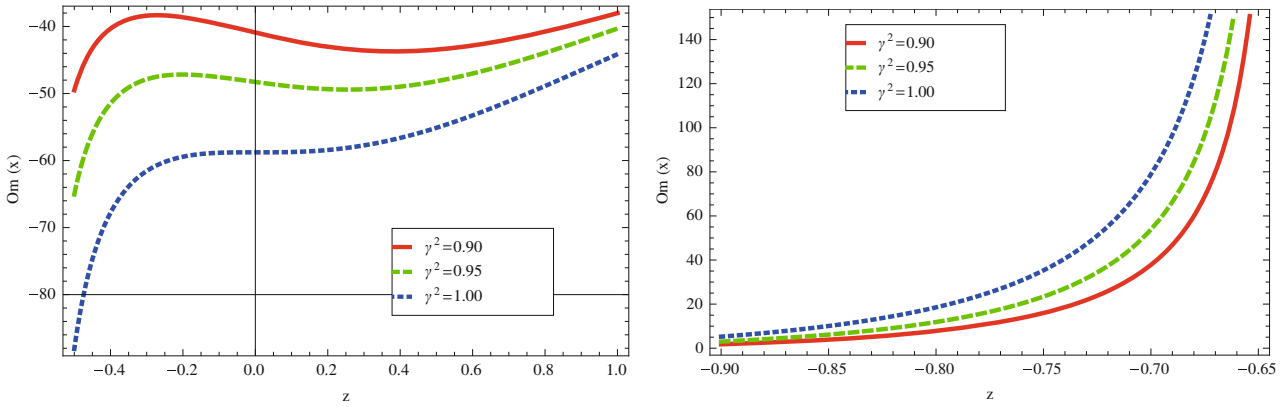

Fig. 3. Plots of Om-diagnostics *versus* z.

Using eq. (17) in the above equation we get

$$Om(x) = \left(\frac{2H_0^2\Omega_{m0}e^{-3(-1+\gamma^2)x}}{3\alpha(1-\gamma^2)+2(1-\beta)} + \frac{b^2e^{-6x}}{18\alpha+6(1-\beta)} + c_1e^{\frac{2x(1-\beta)}{\alpha}} - H_0\right) \times \left(H_0(1-x^3)\right)^{-1}. \tag{20}$$

The plots of Om-diagnostic against z by taking $x = \ln(1+z)^{-1}$ is shown in fig. 3. It can be observed from the right panel of fig. 3 that the trajectories of the Om-diagnostic plane for all γ^2 present positive slopes, which implies phantom behavior. However, the trajectories present negative slopes in the left panel of fig. 3, which represents the quintessence behavior of the universe. This type of behavior of the Om-diagnostic planes show consistency with the EoS parameter and hence with the observational analysis.

4 Cosmological planes

In this section, we discuss cosmological planes, such as ω_ϑ-ω'_ϑ and r-s planes, respectively.

4.1 The ω_ϑ-ω'_ϑ plane

The ω_ϑ-ω'_ϑ plane is used to describe the dynamical property of various DE models. Caldwell and Linder [37] were the first who introduced this method for studying the behavior of quintessence scalar field DE model. They divided the ω_ϑ-ω'_ϑ plane into two regions:

– The thawing region is the region where the EoS parameter evolves from -1, increases with time while its evolution parameter expresses positive behavior, *i.e.*, $\omega'_\vartheta > 0$ for $\omega_\vartheta < 0$.

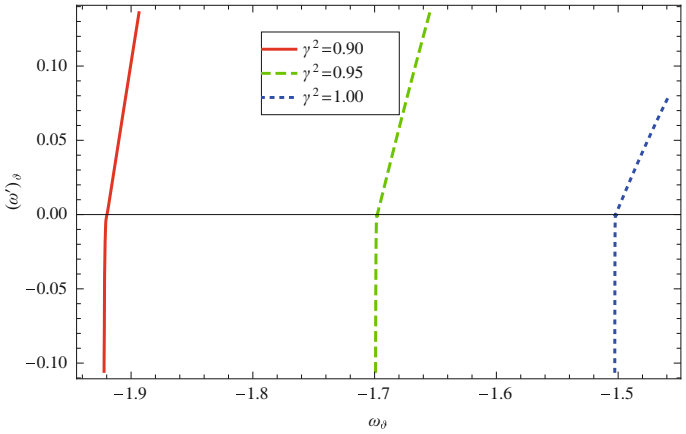

Fig. 4. Plot of ω_ϑ-ω'_ϑ.

– In the freezing region, the evolution parameter remains negative, *i.e.* $\omega'_\vartheta < 0$ for $\omega_\vartheta < 0$.

Taking the derivative of the EoS parameter with respect to $x = \ln a$, we get ω'_ϑ as follows:

$$\omega'_\vartheta = -1 - \left[\frac{-3b^2(3\alpha-\beta)}{2(1+3\alpha-\beta)} + 9e^{\frac{-2x(-1+\beta)}{\alpha}}c_1 + (-1+\frac{2}{2-3(-1+\gamma^2\alpha)-2\beta}) \times 9e^{3(-1+\gamma^2)x}H_0^2\Omega_{m0}\right]^{-1}\left(\frac{-3b^2e^{-6x}(3\alpha-\beta)}{1+3\alpha-\beta} + \frac{6e^{\frac{-2x(1-\beta)}{\alpha}}(-1+\beta)c_1}{\alpha} + 9\gamma^2e^{3(-1+\gamma^2)x}H_0^2\Omega_{m0} + 9(-1+\gamma^2)e^{3(-1+\gamma^2)x}3((-1+\gamma^2)\alpha+2\beta)H_0^2\Omega_{m0} \times \frac{1}{3(-1+\gamma^2)\alpha+2(-1+\beta)}\right) - 9\left[\left(\frac{b^2e^{-6x}(3\alpha-\beta)}{1+3\alpha-\beta} - 2e^{\frac{-2x(-1+\beta)}{\alpha}} \times \frac{(-1+\beta)c_1}{\alpha} - \frac{3(-1+\gamma^2)e^{3(-1+\gamma^2)x}(3(-1+\gamma^2)\alpha+2\beta)H_0^2\Omega_{m0}}{3(-1+\gamma^2)\alpha+2(-1+\beta)}\right) \times \left(\frac{-3b^2e^{-6x}(3\alpha-\beta)}{1+3\alpha-\beta} + \frac{6e^{\frac{-2x(1-\beta)}{\alpha}}(-1+\beta)c_1}{\alpha} + 9\gamma^2e^{3(-1+\gamma^2)x}H_0^2\Omega_{m0} + \frac{9(-1+\gamma^2)e^{3(-1+\gamma^2)x}3((-1+\gamma^2)\alpha+2\beta)H_0^2\Omega_{m0}}{3(-1+\gamma^2)\alpha+2(-1+\beta)}\right)\right]\left(\frac{-3b^2e^{-6x}(3\alpha-\beta)}{1+3\alpha-\beta} + \frac{6e^{\frac{-2x(1-\beta)}{\alpha}}(-1+\beta)c_1}{\alpha} + \frac{9(-1+\gamma^2)e^{3(-1+\gamma^2)x}3((-1+\gamma^2)\alpha+2\beta)H_0^2\Omega_{m0}}{3(-1+\gamma^2)\alpha+2(-1+\beta)} + 9\gamma^2e^{3(-1+\gamma^2)x}H_0^2\Omega_{m0}\right)^{-2} + 3\left[\frac{6b^2e^{-6x}(3\alpha-\beta)}{1+3\alpha-\beta} + 9d^2(-1+\gamma^2)e^{3(-1+\gamma^2)x} \times H_0^2\Omega_{m0} + \frac{9(-1+\gamma^2)^2e^{3(-1+\gamma^2)x}(3(-1+\gamma^2)\alpha+2\beta)H_0^2\Omega_{m0}}{3(-1+\gamma^2)\alpha+2(-1+\beta)} - \frac{4e^{\frac{-2x(-1+\beta)}{\alpha}}}{c_1\alpha^2} \times (-1+\beta)^2\right]\left(\frac{-3b^2e^{-6x}(3\alpha-\beta)}{1+3\alpha-\beta} + \frac{6e^{\frac{-2x(1-\beta)}{\alpha}}(-1+\beta)c_1}{\alpha} + 9\gamma^2e^{3(-1+\gamma^2)x} \times H_0^2\Omega_{m0}\frac{9(-1+\gamma^2)e^{3(-1+\gamma^2)x}3((-1+\gamma^2)\alpha+2\beta)H_0^2\Omega_{m0}}{3(-1+\gamma^2)\alpha+2(-1+\beta)}\right)^{-1}.$$

The ω_ϑ-ω'_ϑ plane for the present scenario has been displayed in fig. 4. The trajectories meet the freezing as well as thawing regions for all cases γ^2.

Moreover, Ade *et al.* [6] have found constraints on w_ϑ and w'_ϑ through observational analyses, which are given as follows:

$$\omega_\vartheta = -1.13^{+0.24}_{-0.25} \quad \text{(Planck+WP+BAO)},$$
$$\omega'_\vartheta < 1.32, \quad \text{(Planck+WP+BAO)},$$

at the 95% confidence level. Also, other data with different combinations of observational schemes, such as (Planck+WP+Union 2.1) and (Planck+WP+SNLS) favor the above constraints. The trajectories of ω'_ϑ against ω_ϑ in our case also lies within the above constraints, which leads to the consistency with the observational constraints.

4.2 Statefinder parameters

Sahni *et al.* [38] proposed statefinder parameters in terms of Hubble as well as deceleration parameters as follows:

$$r = 2q^2 + q - \dot{q}, \qquad s = \frac{r-1}{3(q-\frac{1}{2})},$$

where q is the deceleration parameter and given as

$$q = -1 - \frac{\dot{H}}{H^2}.$$

Using eq. (16) in the above expression, we obtain

$$q = \left(\frac{b^2e^{-6x}}{1+3\alpha-\beta} + \frac{2e^{\frac{-2x(-1+\beta)}{\alpha}}(-1+\beta)}{\alpha} + \frac{6(-1+\gamma^2)e^{-3(-1+\gamma^2)x}H_0^2\Omega_{m0}}{2-3\alpha+3\gamma^2\alpha+2\beta}\right)$$
$$\times\left(\frac{b^2e^{-6x}}{6+18\alpha-6\beta}e^{\frac{-2x(-1+\beta)}{\alpha}}c_1 - \frac{2e^{3(1-\gamma^2)x}}{H}{}^2{}_0\Omega_{m0} - 2-3\alpha+3\gamma^2\alpha+2\beta\right)^{\frac{-3}{2}} - 1,$$

These declaration parameters are geometrically diagnostic because of their total dependence on the expansion factor. The most remarkable points of the (r, s) plane is that we can find the distance of a given DE model from the ΛCDM limit. This defines the well-known regions given below:

- $(r, s) = (1, 0)$ represents the ΛCDM limit;
- $(r, s) = (1, 0)$ represents the CDM limit;
- $r < 1$ and $s > 0$ constitute the quintessence and phantom DE regions;
- $r > 1$ and $s < 0$ give the Chaplygin gas behavior.

Inserting the value of q in eq. (4.2), we obtain

$$r = -1 + \left[\frac{c_1e^{\frac{-2x(-1+\beta)}{\alpha}}(-1+\beta)^2c_1}{\alpha^2} - \frac{18(-1+\gamma^2)^2e^{3(-1+\gamma)x}H_0^2\Omega_{m0}}{3(-1+\gamma^2)\alpha+2(-1+\beta)} + \frac{6b^2e^{-6x}}{1+3\alpha-\beta}\right]\left(\frac{b^2e^{-6x}}{6+18\alpha-6\beta} + e^{\frac{-2x(-1+\beta)}{\alpha}}c_1\right.$$
$$\left.\frac{2e^{3(-1+\gamma^2)x}H_0^2\Omega_{m0}}{2-3\alpha+3\gamma^2\alpha+2\beta}\right)^{\frac{-3}{2}} + \left[\frac{b^2e^{-6x}}{1+3\alpha-\beta} + \frac{2e^{\frac{-2x(-1+\beta)}{\alpha}}(-1+\beta)c_1}{\alpha} + \frac{6(-1+\gamma^2)e^{3(-1+\gamma^2)x}H_0^2\Omega_{m0}}{-2-3\alpha+3\gamma^2\alpha+2\beta}\right]\left(\frac{b^2e^{-6x}}{6+18\alpha-6\beta}\right.$$
$$\left.+e^{\frac{-2x(-1+\beta)}{\alpha}}c_1 - \frac{2e^{3(-1+\gamma^2)x}H_0^2\Omega_{m0}}{2-3\alpha+3\gamma^2\alpha+2\beta}\right)^{\frac{-3}{2}} + 3\left(\frac{-b^2e^{-6x}}{1+3\alpha-\beta} + \frac{2e^{\frac{-2x(-1+\beta)}{\alpha}}(-1+\beta)}{\alpha} - \frac{6(-1+\gamma^2)e^{3(-1+\gamma^2)x}H_0^2\Omega_{m0}}{-2-3\alpha+3\gamma^2\alpha+2\beta}\right)$$
$$\times\left(\frac{-b^2e^{-6x}}{1+3\alpha-\beta} + \frac{6(-1+\gamma^2)e^{3(-1+\gamma^2)x}H_0^2\Omega_{m0}}{-2-3\alpha+3\gamma^2\alpha+2\beta} + \frac{2e^{\frac{-2x(-1+\beta)}{\alpha}}(-1+\beta)}{\alpha}\right)2^{-1}\left[\frac{b^2e^{-6x}}{6+18\alpha-6\beta} + e^{\frac{-2x(-1+\beta)}{\alpha}}c_1\right.$$
$$\left.-\frac{2e^{3(-1+d^2)x}H_0^2\Omega_{m0}}{2-3\alpha+3\gamma^2\alpha+2\beta}\right]^{\frac{-5}{2}} + 2\left[\left(-1+\frac{b^2e^{-6x}}{1+3\alpha-\beta} + \frac{2e^{\frac{-2x(-1+\beta)}{\alpha}}(-1+\beta)c_1}{\alpha} + \frac{6(-1+\gamma^2)e^{3(-1+\gamma^2)x}H_0^2\Omega_{m0}}{-2-3\alpha+3\gamma^2\alpha+2\beta}\right)\right.$$
$$\left.\times\left(\frac{b^2e^{-6x}}{6+18\alpha-6\beta} + e^{\frac{-2x(-1+\beta)}{\alpha}}c_1 - \frac{2e^{3(-1+\gamma^2)x}H_0^2\Omega_{m0}}{2-3\alpha+3\gamma^2\alpha+2\beta}\right)^{\frac{-3}{2}}\right]^2.$$

Subsequently, we can get s as follows:

$$
\begin{aligned}
s = & \Bigg[-2 + \left(\frac{4e^{\frac{-2x(-1+\beta)}{\alpha}}(-1+\beta)^2}{\alpha^2} - \frac{18(-1+\gamma^2)e^{3(-1+\gamma^2)x}H_0^2\Omega_{m0}}{3(-1+\gamma^2)\alpha + 2(-1+\beta)} + \frac{6b^2e^{-6x}}{1+3\alpha-\beta} \right) \\
& + \left(\frac{b^2e^{-6x}}{6+18\alpha-6\beta} + e^{\frac{-2x(-1+\beta)}{\alpha}}c_1 - \frac{2e^{3(-1+\gamma^2)x}H_0^2\Omega_{m0}}{2-3\alpha+3\gamma^2\alpha+2\beta} \right)^{\frac{-3}{2}} \\
& + \left(\frac{b^2e^{-6x}}{1+3\alpha-\beta} + \frac{2e^{\frac{-2x(-1+\beta)}{\alpha}}(-1+\beta)c_1}{\alpha} + \frac{6(-1+\gamma^2)e^{3(-1+\gamma^2)x}H_0^2\Omega_{m0}}{2-3\alpha+3\gamma^2\alpha+2\beta} \right) \\
& + \left(\frac{b^2e^{-6x}}{6+18\alpha-6\beta} + e^{\frac{-2x(-1+\beta)}{\alpha}}c_1 - \frac{2e^{3(-1+\gamma^2)x}H_0^2\Omega_{m0}}{2-3\alpha+3\gamma^2\alpha+2\beta} \right)^{\frac{-3}{2}} \\
& + 3\left(-b^2e^{-6x}(1+3\alpha-\beta)^{-1} - \frac{2e^{\frac{-2x(-1+\beta)}{\alpha}}(-1+\beta)c_1}{\alpha} \right) \\
& - 6\left(-1+\gamma^2e^{3(-1+\gamma^2)x}\frac{H_0^2\Omega_{m0}}{2-3\alpha+3\gamma^2\alpha+2\beta} \right)\left(\frac{b^2e^{-6x}}{1+3\alpha-\beta} + \frac{2e^{\frac{-2x(-1+\beta)}{\alpha}}(-1+\beta)c_1}{\alpha} \right) \\
& + 6\left(\left(-1+\gamma^2e^{3(-1+\gamma^2)x} \right)\frac{H_0^2\Omega_{m0}}{2-3\alpha+3\gamma^2\alpha+2\beta} \right)^2 \left(\frac{b^2e^{-6x}}{6+18\alpha-6\beta} + e^{\frac{-2x(-1+\beta)}{\alpha}}c_1 - \frac{2e^{3(-1+\gamma^2)x}H_0^2\Omega_{m0}}{2-3\alpha+3\gamma^2\alpha+2\beta} \right)^{\frac{-5}{2}} \\
& + 2\left(-1 + \frac{b^2e^{-6x}}{1+3\alpha-\beta} + \frac{2e^{\frac{-2x(-1+\beta)}{\alpha}}}{\alpha}(-1+\beta)c_1 + \frac{6(-1+\gamma^2e^{3(-1+\gamma^2)x}H_0^2\Omega_{m0})}{2-3\alpha+3\gamma^2\alpha+2\beta} \right) \\
& \times \left(\frac{b^2e^{-6x}}{6+18\alpha-6\beta} + e^{\frac{-2x(-1+\beta)}{\alpha}}c_1 - \frac{2e^{3(-1+\gamma^2)x}H_0^2\Omega_{m0}}{2-3\alpha+3\gamma^2\alpha+2\beta} \right)^{\frac{-3}{2}} \Bigg] \\
& \times \Bigg[3\left(\frac{-3}{2} + \frac{b^2e^{-6x}}{1+3\alpha-\beta} + \frac{2e^{\frac{-2x(-1+\beta)}{\alpha}}(-1+\beta)c_1}{\alpha} + \frac{6(-1+\gamma^2)e^{3(-1+\gamma^2)x}H_0^2\Omega_{m0}}{2-3\alpha+3\gamma^2\alpha+2\beta} \right) \\
& \times \left(\frac{b^2e^{-6x}}{6+18\alpha-6\beta} + e^{\frac{-2x(-1+\beta)}{\alpha}}c_1 - \frac{2e^{3(-1+d^2)x}H_0^2\Omega_{m0}}{2-3\alpha+3\gamma^2\alpha+2\beta} \right)^{\frac{-3}{2}} \Bigg].
\end{aligned}
$$

The r-s statefinder plane for the present framework has been depicted in fig. 5 for three different values of γ^2. We can see that only the trajectory of the r-s plane for $\gamma^2 = 1$ meets the ΛCDM limit. The statefinder trajectories constitute the quintessence/phantom region (for $r < 1$ and $s > 0$) for $\gamma^2 = 0.9, 0.95$. Also, the Chaplygin gas behavior (where $s < 0$, $r > 1$) is obtained only for the trajectory for $\gamma^2 = 1$.

5 Conclusion

Recently, Pasqua *et al.* [29] discussed only the solution of the scale factor corresponding to the NHDE model with a non-interacting scenario in the dynamical Chern-Simons modified gravity. We have extended this work by taking the interacting NHDE model in the framework of dynamical Chern-Simons modified gravity with different cosmological parameters. We have explored cosmological parameters (EoS parameter, squared speed of sound parameter and Om-diagnostic) and cosmological planes (ω_ϑ-ω'_ϑ and statefinder), respectively. The EoS parameter ω_ϑ is shown in fig. 1 *versus* z for some constant cosmological parameters. We have found that our results for the EoS parameter are consistent with a combination of various observational data at 95% confidence level by the Planck Collaboration ([6] and references therein). The details are the following:

$$
\begin{aligned}
\omega_\vartheta &= -1.13^{+0.24}_{-0.25} \quad \text{(Planck+WP+BAO)}, \\
\omega_\vartheta &= -1.09 \pm 0.17 \quad \text{(Planck+WP+Union 2.1)}, \\
\omega_\vartheta &= -1.13^{+0.13}_{-0.14} \quad \text{(Planck+WP+SNLS)}, \\
\omega_\vartheta &= -1.24^{+0.18}_{-0.19} \quad \text{(Planck+WP+}H_0\text{)}.
\end{aligned}
$$

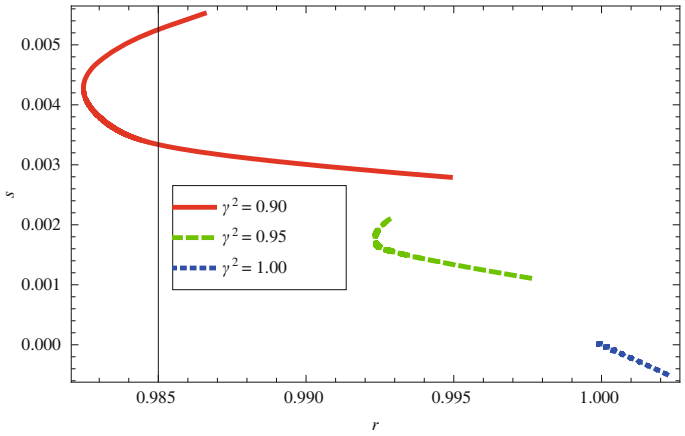

Fig. 5. Plots of the statefinder pair in r-s for different values of γ^2.

We have also observed that the squared speed of sound shows stability of the model at the present epoch as well as later epoch (fig. 2). The plots of the Om-diagnostic against z by taking $x = \ln(1+z)^{-1}$ are shown in fig. 3. It can be observed from the right panel of fig. 3 that the trajectories of the Om-diagnostic plane for all values of γ^2 present positive slopes, which implies phantom behavior. However, the trajectories present negative slopes in the left panel of fig. 3, which represents quintessence behavior of the universe. This type of behavior of Om-diagnostic planes shows consistency with the EoS parameter and hence with observational analyses.

The ω_ϑ-ω'_ϑ plane for the present scenario is displayed in fig. 4. The trajectories meet the freezing as well as thawing regions for all γ^2 cases. Moreover, the ω_ϑ-ω'_ϑ plane is consistent with the following, as obtained through observational data [6]:

$$\omega_\vartheta = -1.13^{+0.24}_{-0.25} \quad \text{(Planck+WP+BAO)},$$
$$\omega'_\vartheta < 1.32 \quad \text{(Planck+WP+BAO)},$$

at 95% confidence level. The r-s statefinder plane for the present framework is depicted in fig. 5 for three different values of γ^2. We can see that the only trajectory of the r-s plane for $\gamma^2 = 1$ meets the ΛCDM limit. The statefinder trajectories constitute the quintessence/phantom region (for $r < 1$ and $s > 0$) for $\gamma^2 = 0.9, 0.95$. Also, the Chaplygin gas behavior (where $s < 0$, $r > 1$) is obtained only for the trajectory for $\gamma^2 = 1$.

Here we provide comparison with some other papers on holographic dark energy model and Chern-Simons gravity. Jawad and Majeed [39] discussed interacting PDE (Hubble horizon as an infrared cutoff) with cold dark matter in flat universe. They developed the EoS paramenter and studied scalar field models in this scenario. Jawad and Rani [40] explored the cosmological evolution of the universe in the framework of Chern-Simons gravity. They considered the pilgrim dark energy (PDE) model with known horizons, like Hubble and event horizons. They also discussed cosmological parameters, such as EoS, ω_θ-ω'_θ and squared speed of sound, which show observationally consistent behavior. Jawad and Sohail in [41] examined the DE scenario in the framework of the modified Chern-Simons gravity by considering QCD ghost DE model. They obtained the analytical solution of the scale factor and found that the EoS parameter and the cosmological planes provide consistent solution. Taking into account the interacting HDE with the new infrared cutoff in non-flat universe, Sharif and Jawad [42] studied the EoS and squared speed of sound parameters. They also found correspondence between this model and some well-known scalar field models including quintessence, tachyon, K-essence and dilaton. These scenarios represent the accelerated expansion of the universe. The validity of the generalized second law of thermodynamics is also discussed for this model.

In the Kaluza-Klein universe, Sharif and Jawad [21] analyzed the interaction of modified HDE with dark matter by considering varying G with the event horizon. They evaluated the EoS parameter and checked the validity of generalized second law of thermodynamics. This model represents the transition of the universe from quintessence to phantom. In the present paper, we have taken the framework of dynamical Chern-Simons gravity with the new HDE model (HDE model with Granda-Oliveros cutoff) having interaction with dust matter. In order to analyze the insights of this model, we explore EoS, squared speed of sound, Om-diagnostic parameters and ω_ϑ-ω'_ϑ, statefinder planes. These are summarized as follows:

- The EoS parameter gives consistent ranges as compared with different observational data.
- The squared speed of sound represents stable behavior.
- The Om-diagnostic describes quintessence as well as phantom eras.
- The ω_ϑ-ω'_ϑ plane gives thawing and freezing regions.
- The statefinder parameters show all possible eras of the evolving universe. universe.

We discussed some graphs for different values of the interaction parameter.

References

1. P. de Bernardis *et al.*, Nature **955**, 404 (2002).
2. A.G. Riess *et al.*, Astron. J. **116**, 1009 (1998).
3. S. Perlmulter *et al.*, Astrophys. J. **517**, 565 (1999).
4. C.L. Bernnelt *et al.*, Astrophys. J. **148**, 1 (2003).
5. Tegmark *et al.*, Astrophys. J. **606**, 702 (2004).
6. Planck Collaboration (P.A.R. Ade *et al.*), Astron. Astrophys. **571**, A16 (2014).
7. S.W. Allen *et al.*, Mon. Not. R. Astron. Soc. **353**, 457 (2004).
8. A.Y. Kamenshchik, U. Moschella, V. Pasquier, Phys. Lett. B **511**, 265 (2001).
9. M.C. Bento, O. Bertolami, A.A. Sen, Phys. Rev. D **66**, 043507 (2002).
10. Q.G. Huang, Y.G. Gong, JCAP **08**, 006 (2004).
11. X. Zhang, F.Q. Wu, Phys. Rev. D **72**, 043524 (2005).
12. L.N. Granda, A. Oliveros, Phys. Lett. B **669**, 275 (2008).
13. H. Wei, Class. Quantum Grav. **29**, 175008 (2012).
14. M. Sharif, A. Jawad, Eur. Phys. J. C **73**, 2382 (2013).
15. M. Sharif, A. Jawad, Eur. Phys. J. C **73**, 2600 (2013).
16. M. Sharif, A. Jawad, Astrophy. Space Sci. **351**, 321 (2014).
17. A. Jawad, Eur. Phys. J. C **74**, 3215 (2014).
18. A. Jawad, S. Rani, Adv. High Ener. Phys. **2015**, 952156 (2015).
19. L. Susskind, J. Math. Phys. **36**, 6377 (1995).
20. A. Cohen, D. Kaplan, A. Nelson, Phys. Rev. Lett. **82**, 4971 (1999).
21. M. Sharif, A. Jawad, Astrophys. Space Sci. **337**, 789 (2012).
22. R. Jackiw, S.Y. Pi, Phys. Rev. D **68**, 104012 (2003).
23. J. Polchinski, *Superstring Theory and Beyond String Theory*, Vol. **2** (Cambridge University Press, Cambridge, 1998).
24. A. Ashtekar, A.P. Balachandran, S. Jo, Int. J. Mod. Phys. A **4**, 1493 (1989).
25. S. Alexander, N. Yunes, Phys. Rep. **480**, 155 (2009).
26. C. Furtado *et al.*, arXiv:1005.1911v3.
27. J.G. Silva, A.F. Santos, Eur. Phys. J. C **73**, 2500 (2013).
28. Y.S. Myung, Eur. Phys. J. C **73**, 2515 (2013).
29. A. Pasqua, R. da Rocha, S. Chattopadhyay, Eur. Phys. J. C **75**, 44 (2015).
30. S. Rani, T. Nawaz, A. Jawad, Astrophys. Space Sci. **361**, 285 (2016).
31. S. Nojiri, S.D. Odintsov, Phys. Rev. D **74**, 086005 (2006).
32. S. Nojiri, S.D. Odintsov, Gen. Relativ. Gravit. **38**, 1285 (2006).
33. S. Nojiri, S.D. Odintsov, J. Phys. Conf. Ser. **66**, 012005 (2007).
34. S. Nojiri, S.D. Odintsov, D. Diego Sáez-Gómez, Phys. Lett. B **681**, 74 (2009).
35. K. Bamba *et al.*, Astrophys. Space Sci. **342**, 155 (2012).
36. V. Sahni, A. Shafieloo, A.A. Starobinsky, Phys. Rev. D **78**, 103502 (2008).
37. R.R. Calldwell, E.V. Linder, Phys. Rev. Lett. **95**, 41301 (2005).
38. V. Sahni *et al.*, JETP Lett. **77**, 201 (2003).
39. A. Jawad, A. Majeed, Astrophy. Space Sci. **356**, 375 (2015).
40. A. Jawad, S. Rani, Adv. High Energy Phys. **2015**, 259578 (2015).
41. A. Jawad, A. Sohail, Astrophys. Space Sci. **359**, 55 (2015).
42. M. Sharif, A. Jawad, Eur. Phys. J. C **72**, 2097 (2012).